

Shooter Localization using a Wireless Sensor Network of Soldier-Worn Gunfire Detection Systems

JEMIN GEORGE
LANCE M. KAPLAN

This paper addresses the problem of shooter localization using a wireless sensor network of soldier-worn gunfire detection systems. If the sensor is within the field of view of the shockwave generated by the supersonic projectile, then using acoustic phenomena analysis, the gunfire detection system can localize the source of the incoming fire with respect to the sensor location. These relative solutions from individual gunfire detection systems are relayed to the central node, where they are fused to yield a highly accurate geo-rectified solution, which is then relayed back to the soldiers for added situational awareness. Detailed formulation of the fusion methodology presented here indicates that the multi-sensor fusion algorithm for soldier-worn gunfire detection systems is essentially a weighted nonlinear least-squares algorithm, which can easily be implemented using the Gauss-Newton method. The performance analysis of the proposed fusion algorithm through numerical simulations reveals that the fused solution is much more accurate compared to the individual best sensor solution and the simple averaged sensor solution. Since the proposed fusion algorithm requires consistent weighting of individual sensor solutions, a consistency-based weighting scheme is introduced to tackle the lack of reliability among sensor provided weights. Implementation of the proposed fusion scheme along with the consistency-based weighting scheme on experimental data further confirms the numerical results.

Manuscript received December 16, 2011; revised May 18, 2012; released for publication September 15, 2012.

Refereeing of this contribution was handled by Benjamin Slocumb.

Author's addresses: J. George and L. M. Kaplan are with the Sensors and Electron Devices Directorate, U.S. Army Research Laboratory, 2800 Powder Mill Rd., Adelphi, MD 20783, E-mail: (jemin.george.civ@mail.mil).

1557-6418/13/\$17.00 © 2013 JAIF

1. INTRODUCTION

Highly accurate small-arms gunfire detection systems on individual soldiers are vital requirement for added battlefield situational awareness and threat assessment. Today, several acoustic shooter localization systems are commercially available [2, 7, 29]; an overview of such systems can be found in [26]. A few examples of soldier-wearable shooter localization systems include the Shoulder-Worn Acoustic Targeting System (SWATS) by QinetiQ North America, Inc., Boomerang Warrior-X by BBN Technologies, and PinPoint by BioMimetic Systems. These Soldier-wearable Gunfire Detection Systems (SW-GDSs) can provide a good level of localization accuracy as long as the soldier is at an ideal location relative to the shooter and the bullet trajectory. However, due to the dissipative nature of acoustic signals, localization systems suffer severe performance degradation as the distance to the shooter and the bullet trajectory increases [22, 23, 28]. Moreover, when a relative solution, i.e., the shooter location relative to the sensor, is transformed into a geo-rectified solution using a magnetometer and GPS, the solution often becomes unusable due to localization errors. Geo-rectified solutions are necessary when displaying hostile fire icons on a Command and Control Geographic Information System (C2 GIS) map display.

SW-GDSs use acoustic phenomena analysis of small-arms fire to localize the source of incoming fire, usually with a bearing and range relative to the user [12]. Currently, the individual SW-GDSs operate separately and are not designed to exploit the sensor network layout of all the soldiers within a Small Combat Unit (SCU) to help increase accuracy. Researchers are exploring some novel solutions that utilize the team aspect of these SCUs by exploiting all SW-GDSs in a squad/platoon to increase detection rates and localization accuracy [9, 10, 32]. Apart from soldier-wearable systems, there exist several single-microphone as well as microphone array-based sensor network approaches to shooter localization [6, 15, 16, 19, 24]. Most of the existing sensor fusion schemes for shooter localization are centralized approaches where the individual sensor measurements, such as time of arrival or angle of arrival of the muzzle blast or the shockwave are combined to yield a single estimate of the shooter position [5, 16, 19, 20, 32]. Here we consider a hierarchical approach where the relative shooter position from the individual sensors are fused to obtain a more accurate geo-rectified shooter position. The proposed approach takes full advantage of the team aspect of a SCU to provide a fused solution that would be more accurate and suitable for a C2 GIS map display than the individual soldier's solution. The objective here is to improve accuracy across an entire SCU so even soldiers in non-ideal settings (out of range, bad angle, etc.) can exploit the good solutions

from their neighbors. Furthermore, the proposed hierarchical approach would allow the individual sensors to operate independently in an event of network failure.

The individual SW-GDS is composed of a passive array of microphones that is able to localize a gunfire event by measuring the direction of arrival for both the acoustic wave generated by the muzzle blast and the shockwave generated by the supersonic bullet [2, 7, 12, 23]. After detecting a gunfire, the individual sensors report their solution along with their orientation and GPS positions to a central node over a communication network. At the central node, the individual sensor solutions are fused along with the GPS positions to yield a highly accurate, geo-rectified solution, which is then relayed back to individual soldiers for added situational awareness.

This paper presents a detailed account of our continuing effort in the field of shooter localization using a wireless sensor network, where the main goal is to develop a fusion algorithm that would work well (compared to the individual sensor solutions) across all the off-the-shelf SW-GDSs and not tailored toward any particular acoustic sensor [3, 9, 10, 13, 30]. Even though the exact details of the measurement process in an acoustic GDS is sensor dependent and may considered as proprietary, a brief description of the shooter localization process is presented in Sections 2 and 3 for completeness. Sections 2 and 3 are not intended to provide a detailed and comprehensive explanation of acoustic gunfire detection process; rather, they are presented as a prologue to the fusion algorithm presented in Section 4 and to point out that even with the most simplistic measurement model, the fusion algorithm amounts to a complex nonlinear optimization problem. Readers who are interested in further details of the shooter localization process are referred to [2], [23], and the references within them.

The sensor fusion scheme presented here is a maximum likelihood approach and since here we consider additive white Gaussian noise, the maximum likelihood estimation problem can be posed as a weighted nonlinear least-squares problem. But due to the interdependence between the latent parameters and the measurement noise covariance, the weighted nonlinear least-squares problem is not readily solvable considering the practical limitations in processing time and capability. Therefore, a variance versus bias trade-off study is conducted to reduce the number of parameters in the optimization problem. Furthermore, the SW-GDSs are designed to provide confidence weights along with their individual solutions. From analyzing the experimental data, it was noticed that the weights provided by the sensors are inconsistent with the individual solution accuracy and therefore, a consistency-based weighting scheme is provided. In summary, compared to the existing literature, the four main contributions of this

manuscript are:

- A detailed formulation of the multi-sensor data fusion scheme for a wireless network of SW-GDSs.
- A variance versus bias trade-off study to reduce the number of parameters in the optimization problem for the real-time implementation of the fusion algorithm.
- A consistency-based weighting scheme to tackle the lack of reliability among the sensor provided weights.
- Experimental results and an in-depth analysis of data obtained from implementing the proposed sensor fusion algorithm for realistic sensor formation.

The structure of this paper is as follows: Section 2 presents the measurement model for the soldier-wearable acoustic sensor nodes. Section 3 presents the localization algorithm that converts the sensor measurements to a shooter position estimate. Details of the central node data fusion and the corresponding nonlinear least-squares problem are given in Section 4. Section 5 presents the results from numerical simulations and Section 6 presents the results obtained from implementing the fusion algorithm on experimental data. Finally, Section 7 concludes the paper and discusses the current research challenges.

2. SENSOR MODEL

Consider a SCU consisting of n individual soldiers equipped with the SW-GDS. In order to set up the problem and develop a sensor model, consider a scenario where there is only one shooter and the SW-GDS receives both the muzzle blast and shockwave. The shooter or the target location and the soldier or the i th sensor location are defined as T and S_i , respectively. For simplicity, the problem is formulated in \mathbb{R}^2 , i.e., $T \equiv [T_x \ T_y]^T \in \mathbb{R}^2$ and $S_i \equiv [S_{i_x} \ S_{i_y}]^T \in \mathbb{R}^2$. Now define the individual range, r_i , and bearing, ϕ_i , between the i th sensor node and the target as

$$r_i = \sqrt{(T_x - S_{i_x})^2 + (T_y - S_{i_y})^2} \quad (1)$$

$$\begin{aligned} \phi_i &= \arctan\left(\frac{T_y - S_{i_y}}{T_x - S_{i_x}}\right) \pm \pi\{-1, 0, 1\} \\ &= 2 \arctan \frac{(T_y - S_{i_y})}{\sqrt{(T_x - S_{i_x})^2 + (T_y - S_{i_y})^2} + (T_x - S_{i_x})}. \end{aligned} \quad (2)$$

REMARK 1 For descriptive simplicity, we consider a constant velocity bullet model while the sensors in reality account for the decelerating bullet speed [2]. Since we are mainly interested in developing an algorithm for SW-GDS fusion as opposed to improving the individual sensor capability, the simplified sensor model is presented only for completeness.

When a gun fires, the blast from the muzzle produces a spherical acoustic wave that can be heard in any direction. The bullet travels at supersonic speeds

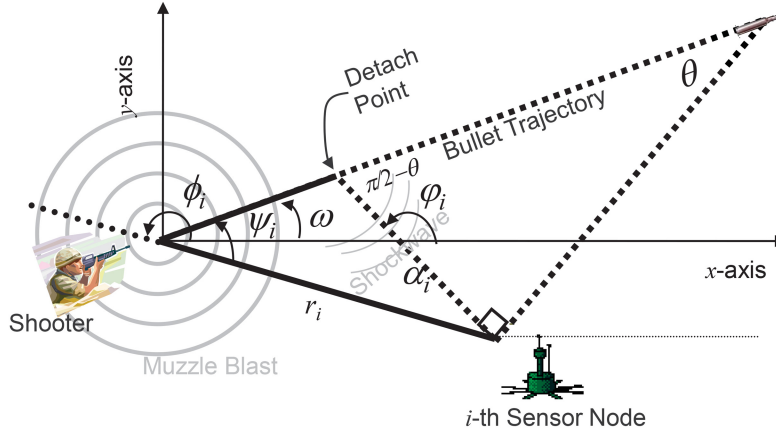


Fig. 1. Geometry of the bullet trajectory and propagation of the muzzle blast and shockwave to the sensor node.

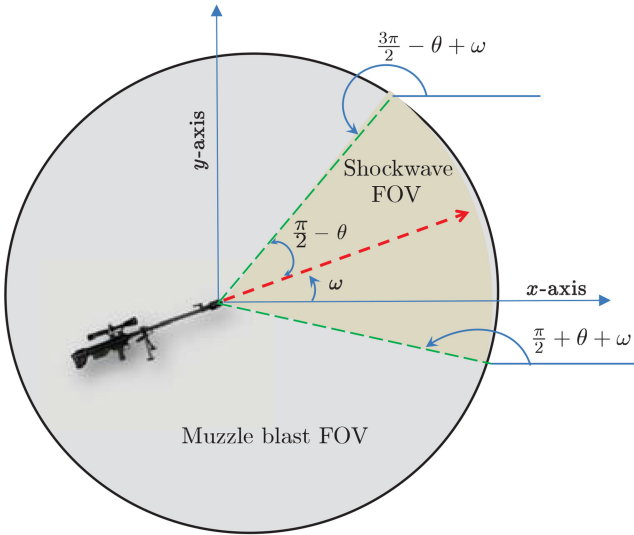


Fig. 2. Muzzle blast and shockwave field of view.

and produces an acoustic shockwave that emanates as a cone from the trajectory of the bullet. Because the bullet is traveling faster than the speed of sound, the shockwave arrives at the sensor node before the wave from the muzzle blast [19], which we simply refer to as the muzzle blast. Figure 1 illustrates the geometry of the shockwave and the muzzle blast for the i th sensor node when the orientation of the bullet trajectory is ω with respect to the horizontal axis. As the bullet pushes air, it creates an impulse wave. The wavefront is a cone whose angle θ with respect to the trajectory is

$$\theta = \arcsin\left(\frac{1}{m}\right) \quad (3)$$

where m is the Mach number [8]. The Mach number is assumed to be known since the typical Mach number for sniper ammunition is $m = 2$.¹ Since the Mach number directly influences the range (distance from the sensor to the shooter) estimates, uncertainty in bullet speed may be treated as a range estimation error.

¹http://www.chuckhawks.com/rifle_ballistics_table.htm.

As indicated in Fig. 1, the angle ϕ_i indicates the direction of arrival (DOA) of the muzzle blast, and φ_i indicates the DOA of the shockwave. The muzzle blast DOA² is measured counter-clockwise such that $0 \leq \phi_i \leq 2\pi$. For a more detailed description of the scenario, please refer to [12]. Figure 2 indicates the field of view (FOV) for both the muzzle blast and the shockwave. Note that the FOV of the muzzle blast is 2π , i.e., omnidirectional, and the FOV for the shockwave is $\pi - 2\theta$. SW-GDS receives the shockwave only if the muzzle blast DOA is within the bounds

$$\pi/2 + \theta + \omega < \phi_i < 3\pi/2 - \theta + \omega. \quad (4)$$

Now, the DOA angle for the shockwave can be written as

$$\varphi_i = \begin{cases} -\frac{\pi}{2} - \theta + \omega, & \text{if } \pi + \omega < \phi_i < \frac{3\pi}{2} - \theta + \omega \\ \frac{\pi}{2} + \theta + \omega, & \text{if } \frac{\pi}{2} + \theta + \omega < \phi_i < \pi + \omega \end{cases}. \quad (5)$$

The first case, $\pi + \omega < \phi_i < (3\pi/2) - \theta + \omega$, corresponds to the scenario where the sensor is located above the bullet trajectory and the second case, $(\pi/2) + \theta + \omega < \phi_i < \pi + \omega$, corresponds to the scenario where the sensor is located below the bullet trajectory (as shown in Fig. 1). The case where $\phi_i = \pi + \omega$ corresponds to the scenario when the sensor is located on the bullet trajectory and we do not consider such a scenario here. If ϕ_i is outside the bounds given in (4), then the sensor node only receives the muzzle blast as it is outside the FOV of the shockwave.

Under the assumptions that the bullet maintains a constant velocity over its trajectory, the time difference of arrival (TDOA) between the shockwave and the muzzle blast can be written as [2]

$$\tau_i = \frac{r_i}{c} [1 - \cos|\phi_i - \varphi_i|], \quad \forall \phi_i \neq \varphi_i \quad (6)$$

²Equation (2) yields $-\pi \leq \phi_i \leq \pi$. Thus π must be added to ϕ_i to obtain a positive ϕ_i if $\phi_i < 0$.

where c indicates the speed of sound. Utilizing (5), the bullet trajectory angle, ω , can be obtained from the shockwave DOA angle. Though this paper assumes that the bullet speed is constant over its trajectory, others have proposed localization algorithms [1], [14], [19] that employ more realistic bullet speed models at the expense of computational efficiency.

When the sensor node is within the FOV of the shockwave, the three available measurements are the two DOA angles and the TDOA between the muzzle blast and the shockwave, i.e.,

$$\hat{\phi}_i = h_1(T, S_i, \omega) + \eta_\phi \quad (7a)$$

$$\hat{\varphi}_i = h_2(T, S_i, \omega) + \eta_\varphi \quad (7b)$$

$$\hat{\tau}_i = h_3(T, S_i, \omega) + \eta_\tau \quad (7c)$$

where $h_1(\cdot)$ is given in (2), $h_2(\cdot)$ is given in (5), and $h_3(\cdot)$ is given in (6). The measurement noise is assumed to be zero mean Gaussian white noise, i.e., $\eta_\phi \sim \mathcal{N}(0, \sigma_\phi^2)$, $\eta_\varphi \sim \mathcal{N}(0, \sigma_\varphi^2)$ and $\eta_\tau \sim \mathcal{N}(0, \sigma_\tau^2)$. Actually, it has been shown that, with the high signal-to-noise ratio, a maximum likelihood DOA estimator is unbiased and its estimates approximately follow a Gaussian distribution [21, 25]. Here (7) represents the measurement equations and after receiving these measurements, the processing capability internal to the individual SW-GDS converts these measurement into shooter location estimates. It is important to note that the typical SW-GDS is equipped with a magnetometer to obtain the orientation of the sensor and thus the DOA measurements are reported in a global reference frame as shown in Fig. 1. Thus, it is not necessary to report the individual sensor orientation to the central node, unless the DOA is given in a local sensor reference frame. Furthermore, assuming the magnetometer measurement errors are Gaussian, the uncertainty associated with the sensor orientation can be simply added to the DOA uncertainty.

3. DATA FUSION AT SENSOR NODE LEVEL

Let \hat{Z}_i denote the individual sensor level estimates on the target bearing, range, and bullet trajectory, i.e., $\hat{Z}_i = [\hat{\phi}_i \ \hat{r}_i \ \hat{\omega}_i]$. Data fusion at the sensor node involves calculating these individual estimates based on the three sensor measurements.

Using (5), the bullet trajectory angle, ω , can be obtained from the shockwave DOA measurements. Thus, the observations on the trajectory angle can be written as

$$\hat{\omega}_i = \omega + \eta_\varphi. \quad (8)$$

Now the likelihood function, $p(\hat{\omega}_i | T, S_i, \omega)$, can be written as

$$p(\hat{\omega}_i | T, S_i, \omega) = \mathcal{N}(\omega, \sigma_\varphi^2).$$

From (6), the range can be written in terms of the TDOA as

$$r_i = \frac{c\tau_i}{[1 - \cos|\phi_i - \varphi_i|]}. \quad (9)$$

The observation of r_i may be written as

$$\hat{r}_i = \frac{c\hat{\tau}_i}{[1 - \cos|\hat{\phi}_i - \hat{\varphi}_i|]}. \quad (10)$$

Using the first-order Taylor series, the range measurement can be approximated as

$$\begin{aligned} \hat{r}_i &\approx \frac{c\tau_i}{[1 - \cos|\phi_i - \varphi_i|]} \\ &+ \left[\frac{c}{[1 - \cos|\phi_i - \varphi_i|]} \quad - \frac{c\tau_i \sin|\phi_i - \varphi_i|}{[1 - \cos|\phi_i - \varphi_i|]^2} \right] \begin{bmatrix} \eta_\tau \\ \eta_{\phi\varphi} \end{bmatrix} \\ &= r_i + H(T, S_i, \omega)\eta_r \end{aligned}$$

where

$$\eta_r = \begin{bmatrix} \eta_\tau \\ \eta_{\phi\varphi} \end{bmatrix}, \quad \eta_{\phi\varphi} \sim \mathcal{N}(0, \sigma_\phi^2 + \sigma_\varphi^2)$$

and

$$H(T, S_i, \omega) = \begin{bmatrix} \frac{c}{[1 - \cos|\phi_i - \varphi_i|]} & - \frac{c\tau_i \sin|\phi_i - \varphi_i|}{[1 - \cos|\phi_i - \varphi_i|]^2} \end{bmatrix}.$$

Now the likelihood $p(\hat{r}_i | T, S_i, \omega)$ can be approximated as

$$p(\hat{r}_i | T, S_i, \omega) \approx \mathcal{N}(r_i, \sigma_r^2(T, S_i, \omega))$$

where the variance $\sigma_r^2(T, S_i, \omega)$ can be written as

$$\sigma_r^2(T, S_i, \omega) = H(T, S_i, \omega) \begin{bmatrix} \sigma_\tau^2 & 0 \\ 0 & \sigma_\phi^2 + \sigma_\varphi^2 \end{bmatrix} H^T(T, S_i, \omega). \quad (11)$$

Thus, the likelihood function $p(\hat{Z}_i | T, S_i, \omega)$ can be approximated as

$$p(\hat{Z}_i | T, S_i, \omega) \approx \mathcal{N}(\mu_{Z_i}, \Sigma_{Z_i}) \quad (12)$$

where

$$\mu_{Z_i} = \begin{bmatrix} \phi_i \\ r_i \\ \omega \end{bmatrix}, \quad \Sigma_{Z_i} = \begin{bmatrix} \sigma_\phi^2 & 0 & 0 \\ 0 & \sigma_r^2(T, S_i, \omega) & 0 \\ 0 & 0 & \sigma_\varphi^2 \end{bmatrix}.$$

It is assumed that a GPS receiver is used to obtain an accurate positioning on each sensor. Thus, the position observation on the sensors are given as

$$\hat{S}_i = \begin{bmatrix} S_{i_x} \\ S_{i_y} \end{bmatrix} + \begin{bmatrix} v_{i_x} \\ v_{i_y} \end{bmatrix} \quad (13)$$

where the noise terms are assumed to be zero mean Gaussian white, i.e., $v_{i_x} \sim \mathcal{N}(0, \sigma_{i_x}^2)$ and $v_{i_y} \sim \mathcal{N}(0, \sigma_{i_y}^2)$. Now the GPS measurement likelihood function may be written as

$$p(\hat{S}_i | S_i) \sim \mathcal{N} \left(\begin{bmatrix} S_{i_x} \\ S_{i_y} \end{bmatrix}, \begin{bmatrix} \sigma_{i_x}^2 & 0 \\ 0 & \sigma_{i_y}^2 \end{bmatrix} \right) \equiv \mathcal{N}(\mu_{S_i}, \Sigma_{S_i}). \quad (14)$$

Assumption 1 Without loss of generality, it can be assumed that the GPS observations on sensor position are independent of target location, observations on

target location, and the projectile trajectory information, i.e.,

$$p(\hat{S}_i | S_i) = p(\hat{S}_i | T, S_i, \omega) = p(\hat{S}_i | \hat{Z}_i, T, S_i, \omega).$$

Based on Assumption 1, the joint probability $p(\hat{Z}_i, \hat{S}_i | T, S_i, \omega)$ can be calculated as

$$p(\hat{Z}_i, \hat{S}_i | T, S_i, \omega) = p(\hat{S}_i | \hat{Z}_i, T, S_i, \omega) p(\hat{Z}_i | T, S_i, \omega). \quad (15)$$

Substituting (12) and (14), the above joint likelihood can be written as

$$p(\hat{Z}_i, \hat{S}_i | T, S_i, \omega) \approx \mathcal{N}(\mu_{S_i}, \Sigma_{S_i}) \mathcal{N}(\mu_{Z_i}, \Sigma_{Z_i}). \quad (16)$$

Now for a sensor located in the FOV of the shockwave, the target location can be estimated as

$$\hat{T}_{x_i} = \hat{S}_{i_x} + \hat{r}_i \cos(\hat{\phi}_i) \quad (17)$$

$$\hat{T}_{y_i} = \hat{S}_{i_y} + \hat{r}_i \sin(\hat{\phi}_i). \quad (18)$$

When the sensor is located outside the shockwave FOV, the only estimate would be the bearing angle. After individual estimates are obtained at the sensor node level, the measured information is transmitted to a central node where it is fused to obtain a more accurate estimate of shooter location.

4. DATA FUSION AT THE CENTRAL NODE

While sensors in the FOV of the muzzle blast and the shockwave yield a range, bearing, and trajectory angle estimates, the gunfire detection systems outside the FOV of the shockwave yield a muzzle blast DOA. Also, GPS measurements are available on each sensor locations. At the central node, this information from the individual sensor nodes is fused to obtain an accurate estimate of the shooter location, bullet trajectory angle, and sensor locations.

Based on Assumption 1, the joint likelihood function associated with each sensor is given in (15). Let $\mathbf{S}_{1:n} = \{S_1, S_2, \dots, S_n\}$, $\hat{\mathbf{Z}}_{1:n} = \{\hat{Z}_1, \hat{Z}_2, \dots, \hat{Z}_n\}$, and $\hat{\mathbf{S}}_{1:n} = \{\hat{S}_1, \hat{S}_2, \dots, \hat{S}_n\}$, where n indicates the number of sensors. Since the measurement errors for the sensor nodes are independent of each other, the joint conditional density $p(\hat{\mathbf{Z}}_{1:n}, \hat{\mathbf{S}}_{1:n} | T, \mathbf{S}_{1:n}, \omega)$ can be defined as

$$p(\hat{\mathbf{Z}}_{1:n}, \hat{\mathbf{S}}_{1:n} | T, \mathbf{S}_{1:n}, \omega) = \prod_{i=1}^n p(\hat{Z}_i, \hat{S}_i | T, S_i, \omega). \quad (19)$$

In the maximum likelihood estimation approach considered here, estimates of the sensor locations, shooter location, and bullet trajectory angle are obtained so that the joint log-likelihood function is maximized, i.e.,

$$\begin{aligned} & \max_{T, \mathbf{S}_{1:n}, \omega} \ln \{ p(\hat{\mathbf{Z}}_{1:n}, \hat{\mathbf{S}}_{1:n} | T, \mathbf{S}_{1:n}, \omega) \} \\ & \Rightarrow \max_{T, \mathbf{S}_{1:n}, \omega} \sum_{i=1}^n \ln \{ p(\hat{Z}_i, \hat{S}_i | T, S_i, \omega) \}. \quad (20) \end{aligned}$$

Based on the results given in the previous section, the criteria for the maximum likelihood estimation can be written as

$$\max_{T, \mathbf{S}_{1:n}, \omega} \sum_{i=1}^n [\ln \{ \mathcal{N}(\mu_{Z_i}, \Sigma_{Z_i}) \} + \ln \{ \mathcal{N}(\mu_{S_i}, \Sigma_{S_i}) \}]. \quad (21)$$

Note that the density $\mathcal{N}(\mu_{Z_i}, \Sigma_{Z_i})$ may be written as

$$\mathcal{N}(\mu_{Z_i}, \Sigma_{Z_i}) = \frac{1}{\sqrt{|2\pi\Sigma_{Z_i}|}} \exp \left\{ -\frac{1}{2} (\hat{Z}_i - \mu_{Z_i})^T \Sigma_{Z_i}^{-1} (\hat{Z}_i - \mu_{Z_i}) \right\} \quad (22)$$

where μ_{Z_i} and Σ_{Z_i} are the same quantities given in (12) if the sensor is within the FOV of the shockwave and

$$\mu_{Z_i} = \phi_i = h_1(T, S_i, \omega), \quad \Sigma_{Z_i} = \sigma_\phi^2$$

if the sensor is outside the FOV of the shockwave. The density $\mathcal{N}(\mu_{S_i}, \Sigma_{S_i})$ is given as

$$\mathcal{N}(\mu_{S_i}, \Sigma_{S_i}) = \frac{1}{\sqrt{|2\pi\Sigma_{S_i}|}} \exp \left\{ -\frac{1}{2} (\hat{S}_i - \mu_{S_i})^T \Sigma_{S_i}^{-1} (\hat{S}_i - \mu_{S_i}) \right\} \quad (23)$$

where

$$\mu_{S_i} = \begin{bmatrix} S_{i_x} \\ S_{i_y} \end{bmatrix}, \quad \Sigma_{S_i} = \begin{bmatrix} \sigma_{i_x}^2 & 0 \\ 0 & \sigma_{i_y}^2 \end{bmatrix}.$$

After substituting (22) and (23) into (21), the maximum likelihood criteria may be written as

$$\begin{aligned} & \min_{T, \mathbf{S}_{1:n}, \omega} \sum_{i=1}^n \left[\frac{1}{2} (\hat{Z}_i - \mu_{Z_i})^T \Sigma_{Z_i}^{-1} (\hat{Z}_i - \mu_{Z_i}) \right. \\ & \quad \left. + \frac{1}{2} (\hat{S}_i - \mu_{S_i})^T \Sigma_{S_i}^{-1} (\hat{S}_i - \mu_{S_i}) \right. \\ & \quad \left. + \ln \left\{ \sqrt{|2\pi\Sigma_{Z_i}|} \right\} + \ln \left\{ \sqrt{|2\pi\Sigma_{S_i}|} \right\} \right]. \quad (24) \end{aligned}$$

Note that the term, $\ln \{ \sqrt{|2\pi\Sigma_{Z_i}|} \}$, in above equation is present due to the fact that Σ_{Z_i} is a function of T , \mathbf{S} , and ω . The last term, $\ln \{ \sqrt{|2\pi\Sigma_{S_i}|} \}$ can be ignored since Σ_{S_i} is a known constant matrix. Since Σ_{Z_i} is assumed to be a diagonal matrix, (24) can be rewritten as

$$\begin{aligned} & \min_{T, \mathbf{S}_{1:n}, \omega} \sum_{i=1}^n \left[\ln(\sigma_{r_i}) + \frac{1}{2} (\hat{Z}_i - \mu_{Z_i})^T \Sigma_{Z_i}^{-1} (\hat{Z}_i - \mu_{Z_i}) \right. \\ & \quad \left. + \frac{1}{2} (\hat{S}_i - \mu_{S_i})^T \Sigma_{S_i}^{-1} (\hat{S}_i - \mu_{S_i}) \right]. \quad (25) \end{aligned}$$

Apart from the initial term, $\ln(\sigma_r)$, the optimization problem given in (25) is similar to that used in the weighted nonlinear least-squares. Thus, the maximum likelihood approach presented here is similar to the weighted nonlinear least-squares estimation.

There exists no closed form solution to the nonlinear least-squares optimization problem given in (25) and therefore a numerical approach must be used. A few

common approaches to solve the nonlinear least-squares problem include the Gauss-Newton method, Nelder-Mead simplex method, and Levenberg-Marquardt method [4]. Almost all these approaches are iterative methods that require an initial approximation to the unknown parameters and provide successively better approximations. The iterative process is repeated until the parameters do not change to within specified limits. Here we mainly utilize the Gauss-Newton method for solving the nonlinear least-squares problem given in (25). The main advantage of the Gauss-Newton method is that it exhibits a “quadratic convergence,” which, simply put, means that the uncertainty in the parameters after $p + 1$ iterations is proportional to the square of the uncertainty after p iterations. Once these uncertainties begin to get small, they decrease quite rapidly. An additional advantage of the Gauss-Newton method is that it only requires calculating the first-order derivatives. Even though one of the major problems with the Gauss-Newton method is that it sometimes diverges if the initial approximation is too far from truth, in the sensor fusion applications, the Gauss-Newton method can be easily initialized using the median of the individual sensor solutions.

4.1. Parameter Reduction

One of the major problems with the real-time implementation of the proposed fusion scheme is that it is a $(2n + 3) - D$ problem and its dimensionality increases as the number of sensors increases. Given in this subsection is an analysis that will help to reduce the dimensionality of the optimization problem.

Most of the SW-GDSs currently available are designed so that they provide the shooter location relative to the sensor location. Moreover, some sensors also provide the weights or the confidence numbers that indicate the estimated accuracy level of the relative solution. These confidence numbers can be used to weight the measurements in the nonlinear least-squares estimation problem given in (25). Thus, (25) can be rewritten as

$$\min_{T, S_{i:n}} \sum_{i=1}^n \left[\frac{1}{2} (\hat{Z}_i - \mu_{Z_i})^T W_i (\hat{Z}_i - \mu_{Z_i}) + \frac{1}{2} (\hat{S}_i - \mu_{S_i})^T \Sigma_{S_i}^{-1} (\hat{S}_i - \mu_{S_i}) \right] \quad (26)$$

where

$$\hat{Z}_i = \begin{bmatrix} \hat{\phi}_i \\ \hat{r}_i \end{bmatrix}$$

$$\mu_{Z_i} = \begin{bmatrix} 2 \arctan \frac{(T_y - S_{iy})}{\sqrt{(T_x - S_{ix})^2 + (T_y - S_{iy})^2} + (T_x - S_{ix})} \\ \sqrt{(T_x - S_{ix})^2 + (T_y - S_{iy})^2} \end{bmatrix}$$

$$W_i = \begin{bmatrix} \frac{1}{\sigma_{\phi_i}^2} & 0 \\ 0 & \frac{1}{\sigma_{r_i}^2} \end{bmatrix}$$

$$\hat{S}_i = \begin{bmatrix} \hat{S}_{ix} \\ \hat{S}_{iy} \end{bmatrix}$$

$$\mu_{S_i} = \begin{bmatrix} S_{ix} \\ S_{iy} \end{bmatrix}.$$

Since the SW-GDS do not report the bullet trajectory, $\hat{\omega}_i$ is not included in \hat{Z}_i . Also,

$$\Sigma_{S_i} = \begin{bmatrix} \sigma_{ix}^2 & 0 \\ 0 & \sigma_{iy}^2 \end{bmatrix}$$

is assumed to be a known matrix and W_i s indicate the weights reported by the sensors. The nonlinear least-squares problem given in (26) is of dimension $2n + 2$. If the sensor reported GPS positions are taken as absolute truth, then the nonlinear least-squares problem given in (26) becomes two dimensional and it may be rewritten as

$$\min_T \sum_{i=1}^n \left[\frac{1}{2} (\hat{Z}_i - \mu_{Z_i})^T W_i (\hat{Z}_i - \mu_{Z_i}) \right]. \quad (27)$$

Note that the problem given in (26) involves estimating more parameters compared to the problem in (27). Thus, based on the arguments given in [11], it can be shown that the Cramér-Rao lower bound for the latter is always less than the lower bound for the former, i.e., the problem in (26) yields higher variance for the shooter location compared to the problem in (27). On the other hand, the low dimensional problem in (27) yields biased estimates since it considers the GPS measurements as absolute truth. This bias grows as GPS errors increases. For small errors, the bias is small so that (27) is more accurate than (26) due to the lower variance. Once the GPS errors exceed a threshold, the bias dominates and (26) becomes more accurate. Simulations in the next section help to determine this threshold.

4.2. Weighting Scheme

It is well known that the performance of the least-squares problems given in (26) and (27) depends on the weights associated with each measurements. The fusion scheme presented earlier assumes that the sensors are designed to provide these weights along with its relative shooter position estimates. These weights indicate the estimated accuracy level of the calculated range and bearing. From analyzing the experimental data, it was noticed that the weights provided by the sensors are inconsistent with the relative solution accuracy. This inconsistency is particularly visible in the case of outliers. Using these inconsistent weights in the fusion process would bias the fused solution toward an outlier. Thus, we provide an ad hoc weighting scheme, which is based on a consistency check, i.e., the weight is selected based on how consistent a particular sensor solution is to the rest of the relative solutions. Recently, several consistency-function-based source localization

algorithms have been proposed, which can provide accurate solutions even if a large number of independent outliers are present in a measurement set [17, 18, 31]. Here, the consistency check is conducted by comparing the individual sensor solution to the fused solution obtained by combining the remaining individual sensor measurements. To this end, we first consider the entire n measurement set and remove the particular sensor measurement for which we would like to generate the weight. Let $\hat{\mathbf{Z}}_{1:n}$ indicate the set of all n sensor measurements and $\hat{\mathbf{Z}}_{1:n}^{(j)}$ indicate the set of measurements excluding the j th sensor measurement. Now we obtain a fused solution, $T^{(j)}$, by combining the remaining $n-1$ measurements, $\hat{\mathbf{Z}}_{1:n}^{(j)}$, after equally weighting them, i.e.,³

$$T^{(j)} = \min_T \sum_{i=1, i \neq j}^n \frac{1}{2} \left(\left[\begin{array}{c} 2 \arctan \frac{(T_y - S_{iy})}{\sqrt{(T_x - S_{ix})^2 + (T_y - S_{iy})^2} + (T_x - S_{ix})} \\ \sqrt{(T_x - S_{ix})^2 + (T_y - S_{iy})^2} \end{array} \right] - \begin{bmatrix} \hat{\phi}_i \\ \hat{r}_i \end{bmatrix} \right)^T \begin{bmatrix} W_{11} & W_{12} \\ W_{12} & W_{22} \end{bmatrix} \\ \times \left(\left[\begin{array}{c} 2 \arctan \frac{(T_y - S_{iy})}{\sqrt{(T_x - S_{ix})^2 + (T_y - S_{iy})^2} + (T_x - S_{ix})} \\ \sqrt{(T_x - S_{ix})^2 + (T_y - S_{iy})^2} \end{array} \right] - \begin{bmatrix} \hat{\phi}_i \\ \hat{r}_i \end{bmatrix} \right) \quad (28)$$

where

$$W = \begin{bmatrix} W_{11} & W_{12} \\ W_{12} & W_{22} \end{bmatrix}$$

is the weight matrix. After obtaining the fused solution, it is then converted into relative range and bearing solutions, $r^{(j)}$ and $\phi^{(j)}$, using the sensor GPS measurements.

$$\begin{bmatrix} \phi^{(j)} \\ r^{(j)} \end{bmatrix} = \begin{bmatrix} 2 \arctan \frac{(T_y - S_{iy})}{\sqrt{(T_x - S_{ix})^2 + (T_y - S_{iy})^2} + (T_x - S_{ix})} \\ \sqrt{(T_x^{(j)} - S_{ix})^2 + (T_y^{(j)} - S_{iy})^2} \end{bmatrix}. \quad (29)$$

Now, the difference between the fused relative solution and the measured relative solution is calculated.

$$E_r^{(j)} = (r^{(j)} - \hat{r}_j)^2 \quad (30)$$

$$E_\phi^{(j)} = (\phi^{(j)} - \hat{\phi}_j)^2. \quad (31)$$

If the individual solution is very close to the fused solution, then it is of high consistency and a large weight is selected. Conversely, if the individual solution is far from the fused solution, then it is of low consistency and a low weight is selected. Thus, the weight are

obtained as

$$W_j = \begin{bmatrix} \frac{1}{E_r^{(j)}} & 0 \\ 0 & \frac{1}{E_\phi^{(j)}} \end{bmatrix}. \quad (32)$$

This procedure is repeated n time so that a consistency-based weight is obtained for the entire n -sensor measurements.

5. NUMERICAL SIMULATIONS

This section presents numerical simulations to assess the localization improvement due to the proposed fusion algorithm. For the simulation scenario considered here, we assume that there are five sensor nodes and the node

locations in meters are

$$\mathbf{S} = \begin{bmatrix} 127 & 20 & 90 & 136 & 182 \\ 107 & 22 & 0 & 68 & 59 \end{bmatrix}.$$

For simplicity, we assume a constant velocity model for the bullet. Thus, the Mach number is selected to be $m = 2$ and the speed of sound is selected to be $c = 342$ m/sec. The measurement noise models are selected as $\sigma_{i_x} = \sigma_{i_y} = 5$ m, $\sigma_\phi = \sigma_\varphi = 4^\circ$, and $\sigma_\tau = 1$ msec. Since there exist several approaches to solve the nonlinear least-squares problem, two different methods are used to obtain solutions for both simulation scenarios. In the first method, the optimization problem is solved using the Gauss-Newton method [4] mentioned in the previous section. The second approach uses the Nelder-Simplex algorithm [27], i.e., the *fminsearch* function in Matlab. Both algorithms are initialized using the median of the sensor-reported shooter location.

For simulation, the shooter is assumed to be located at $T = [50 \text{ m } 50 \text{ m}]^T$ and we select the bullet trajectory to be $\omega = 30^\circ$. Figure 3 shows the first simulation scenario. Due to the sensor locations, the second and the third sensors do not receive the shockwave.

5.1. Simulation Results I

The simulation results presented in this subsection corresponds to the results obtained from solving the full dimensional problem given in (25), where the bullet trajectory as well as the sensor locations are estimated

³The arctangent formulation given in (28) is equivalent to the atan2 function in Matlab and it has a range of $[-\pi, \pi]$.

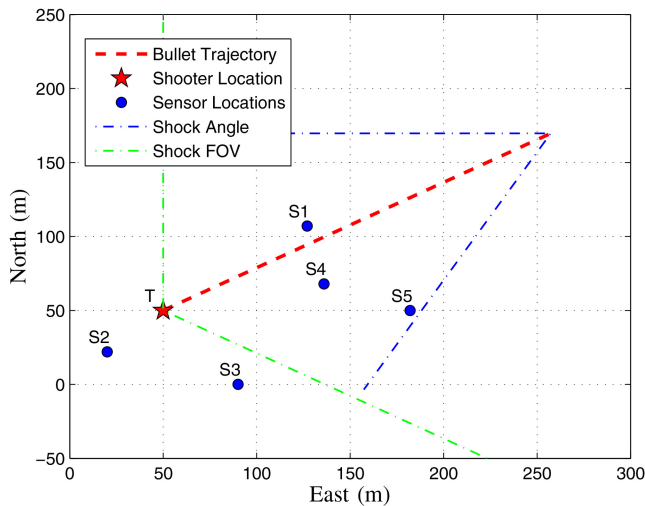


Fig. 3. Simulation I Scenario.

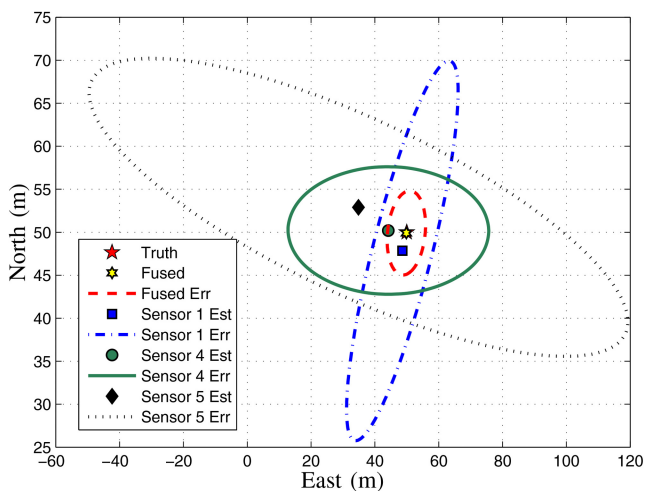


Fig. 4. Simulation result I: Mean results from Monte Carlo runs.

along with the shooter location. In order to evaluate the system performance, 1000 Monte Carlo simulations are conducted for both the Gauss-Newton method and the simplex algorithm. The mean shooter locations and the associated error ellipses obtained from the Monte Carlo simulations using the Gauss-Newton method are given in Fig. 4. A separate plot is not provided for the results obtained using the simplex algorithm since they are very similar to those obtained for the Gauss-Newton method. Figure 4 indicates that sensor five performs the worst out of the three sensors within the shockwave FOV; this is due to the fact that the localization accuracy is inversely proportional to the miss distance. Figure 4 also indicates that the fused estimate is superior to the individual sensor estimates, and the uncertainty associated with the fused estimates is much less than the uncertainty associated with the individual sensor estimates. It seems that the orientation of the error ellipse depends on what side of the trajectory the sensor is located. In addition, the orientation of the error ellipse indicates that the estimation error along the x and y directions varies with the sensor location.

TABLE I
Simulation Result I: Shooter Location

	T_x (m)	T_y (m)	RMSE (m)
Truth	50	50	—
Sensor 1	48.3513	47.2948	23.2870
Sensor 2	—	—	—
Sensor 3	—	—	—
Sensor 4	42.9248	50.2141	31.1132
Sensor 5	37.1197	52.0782	65.6542
Average	42.7986	49.8623	25.9660
Gauss-Newton	49.9066	49.9134	6.8639
Nedler-Simplex	50.0493	50.0588	6.9972

TABLE II
Simulation Result I: Bullet Trajectory

	ω (deg)	RMSE (deg)
Truth	30	—
Sensor 1	30.0641	3.9690
Sensor 2	—	—
Sensor 3	—	—
Sensor 4	30.3402	3.9970
Sensor 5	29.9591	3.9029
Average	30.1211	2.2128
Gauss-Newton	30.1211	2.2128
Nedler-Simplex	30.1999	2.4674

TABLE III
Simulation Result I: Sensor Location RMSE

	GPS (m)	Gauss-Newton (m)	Nedler-Simplex (m)
Sensor 1	7.0215	6.5453	6.5938
Sensor 2	7.0002	6.3195	6.3530
Sensor 3	7.0028	6.6513	6.6770
Sensor 4	7.1509	6.5259	6.6201
Sensor 5	7.0223	6.7883	6.8731

Table I summarizes the mean shooter location estimate of the individual sensors and the fusion algorithms over the Monte Carlo runs. The “average” estimate presented in Table I indicates the estimate obtained by simply averaging the individual target estimates from sensors one, four, and five. Table I also contains the root-mean-square error (RMSE) associated with each estimate. Based on the RMSE presented in Table I, one can conclude that that fused estimates outperform the individual sensors and the simple average estimate.

Table II contains the mean bullet trajectory angle estimate obtained from the individual sensors and the fusion algorithms over the Monte Carlo runs. Table II also contains the RMSE associated with each trajectory angle estimate. Note that the fused trajectory estimate is simply the average of the individual sensor estimates due to the way in which ω appears in (25).

Table III contains RMSE associated with the sensor location estimates. The performance improvement in sensor location estimate accuracy is moderate compared

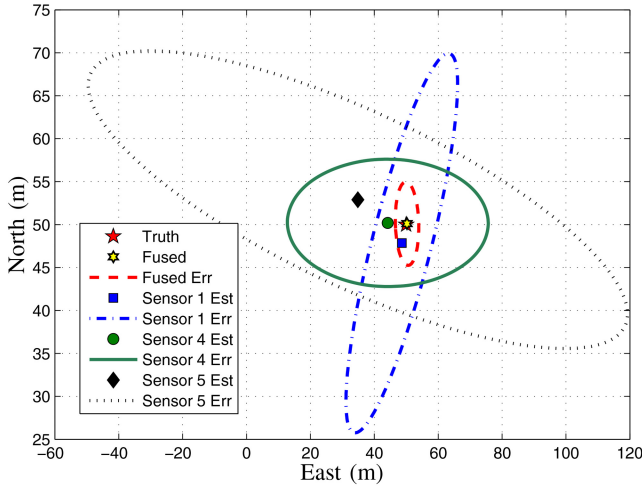


Fig. 5. Simulation result II: Mean results from Monte Carlo runs.

to the shooter location estimate accuracy since the GPS measurements are fairly accurate to begin with. Also note that the RMSE associated with the sensor location estimate given in Table III is similar to that of the RMSE associated with the fused shooter position estimate. Based on the RMSE presented in Tables I, II, and III, one can conclude that that fused estimates outperform the individual sensors.

5.2. Simulation Result II

The simulation results presented in this subsection corresponds to the results obtained from solving the two-dimensional problem given in (27), where only the shooter location is estimated. The mean shooter locations and the associated error ellipses obtained from the Monte Carlo simulation using the Gauss-Newton method are given in Fig. 5. Figure 5 indicates that the error ellipse obtained for the second simulation is smaller compared to that obtained for the first simulation. Also note that the increase in estimation accuracy is mostly along the x -direction, i.e., east. This is due to the fact that the initial error in x -direction is much larger compared to that in y -direction (north). The RMSE associated with the fused result in Fig. 5 is approximately 5.1771 m.

This performance improvement in the low-dimensional problem is due to the very low GPS bias compared to the shooter location estimation error. It can be shown that, as the GPS accuracy decreases, the performance degradation of the $2-D$ problem is much larger compared to that of the full-dimensional problem. Figure 6 compares the RMSE for the shooter location for both the $2-D$ problem given in (27) and the $(2n+2)-D$ problem given in (26). This particular result is obtained for the simulation scenario given in Fig. 3 using additive Gaussian white noise for measurement noise. Figure 6 indicates that for low GPS error of $\sigma_{x,y} \leq 7$ m, the $2-D$ problem yields better accuracy compared to the $(2n+2)-D$ problem. Moreover, for high GPS error of

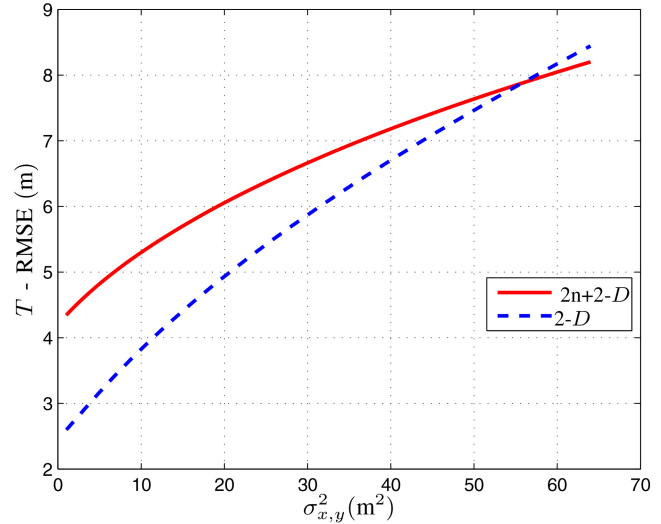


Fig. 6. RMSE sensitivity plot for simulation one scenario.

$\sigma_{x,y} \geq 7.5$ m, taking the GPS measurements as absolute truth and not accounting for the GPS error degrades the shooter location accuracy.

6. EXPERIMENTAL RESULTS

This section presents the experimental results obtained by implementing the fusion algorithm on gunfire detection data, but first, the experimental setup used for data collection is briefly explained. Experimental data were obtained using several gunfire detection systems provided by BioMimetic Systems.⁴ For data collection, we used three soldier-wearable (SW) systems, three unattended ground sensors (UGSs), and three vehicle-mounted (VM) systems.

Each sensor unit had an interface unit attached, consisting of an Atom processor netbook, an Enhanced Position Location and Reporting System (EPLRS) radio, a GPS system, and an Li-145 battery. The netbook was interfaced to the sensor through a custom driver, using serial communication over USB. A standard USB to USB mini cable was used as the interface cable. The netbook was used as a stand-in for the soldier computer; the netbook has the same processor and was an inexpensive substitute for testing. At the central node, the fusion processor receives the solutions from individual sensors via EPLRS radio. The central processor is also an Atom processor netbook where the fusion algorithm combines the individual solutions to obtain a fused solution. The fused solution is then relayed back to individual sensors via EPLRS radio. At the individual sensor nodes, GIS map display is used to display the geo-rectified fused solution.

Experiments were conducted for two sensor formations, the quad symmetric formation and the wedge flank formation. Figure 7 contains the sensor layout for both scenarios. The test pattern includes nine sensors,

⁴www.biomimetic-systems.com.



(a)



(b)

TABLE IV
Shooter Locations

Shooter Position	GPS-East (m)	GPS-North (m)
Shooter Position 1	283309	4709539
Shooter Position 2	283270	4709567
Shooter Position 3	283337	4709632

TABLE V
Ammunition

Weapon	Caliber	Weight (g)	Muzzle Velocity (m/sec)	Velocity at 183 m (m/sec)
Weapon 1	7.62 × 39 mm	124	721	543
Weapon 2	5.56 × 45 mm	55	988	702
Weapon 3	7.62 × 54 mm	181	823	668

three VM sensors (VM-blue), three SW sensors (SW-red), and three UGSs (UGS-green). The sensor pattern is an aggregate distribution of squad-level soldiers while on patrol, it spreads over 25 m front to back. The shooter position is marked by a red human figure, and the shot line is marked by a translucent red line.

For both sensor layouts, shots were fired from three different positions using three different weapons. Figure 7 also shows the three different shooter positions used for the experiment. As Fig. 7 indicates, shooter positions one and two are approximately 200 m from the sensor formation and shooter position three is about 300 m from the sensor formation. The GPS locations of the three shooter positions are given in Table IV. The three different weapons used for the experiment

and details of the ammunition used in the weapons are given in Table V.⁵ For each scenario/shooter position, 10 shots were fired using each weapon. Thus, a total of 180 shots were fired, 60 shots per weapon.

6.1. Results

This subsection presents the summary of experimental results obtained by implementing the fusion algorithm on the gunfire detection data. Before we proceed further, it is important to note that the sensor GPS accuracy level is much higher than the fused solution accuracy, and estimating the sensor position along with

⁵http://www.chuckhawks.com/rifle_ballistics_table.htm.

the shooter location and bullet trajectory does not improve the fused solution accuracy. This is clearly visible in both simulations presented in the previous section, where the fused solution accuracy is very close to the GPS measurement accuracy for the first simulation and the fused solution accuracy is much lower than the GPS accuracy for the second simulation. Besides, including the sensor location as well as the bullet trajectory within the fusion algorithm significantly increases the problem dimensionality and thus contributes to the computational cost. Therefore, the fusion approach used for the experiment does not try to estimate the bullet trajectory and sensor locations based on the results presented in Section 4.1. The sensor locations reported by the sensor GPS is taken as the absolute truth. Thus, the 2-D non-linear least-squares problem associated with the sensor fusion is similar to that given in (27).

As mentioned earlier, the sensors are designed to provide these weights along with its relative shooter position estimates. These weights indicate the estimated accuracy level of the calculated range and bearing. From analyzing the experimental data, it was noticed that the weights provided by the sensors are inconsistent with the relative solution accuracy. This inconsistency is particularly visible in the case of outliers. Using these inconsistent weights in the fusion process would bias the fused solution toward an outlier. Thus, we implemented the fusion algorithm using three different weighting schemes. The first weighting scheme simply uses the weights provided by the sensors; this fusion scheme is denoted as “Fusion-SW (Fusion-Sensor Weights).” For the particular sensor under consideration, the sensor provided weights are obtained based on the signal-to-noise ratio.

The second weighting scheme involves calculating the weights based on the true error associated with the range and bearing estimates; this fusion scheme is denoted as “Fusion-TE (True Error).” For this weighing scheme, the difference between the measured range/bearing and the ground truth are first calculated. The square of these errors are then taken as the weight associated with the range and the bearing measurements. Note that this weighting scheme is not practical in reality since the ground truth is unknown. We use this weighting scheme strictly for comparative purposes. The third weighting scheme is the consistency-based weighing scheme presented in Subsection 4.2 and is denoted as “Fusion-CW (Fusion-Consistency Weights).”

Given next are the results obtained from implementing the fusion algorithm on experimental data. Five different fused solutions are presented per scenario/shooter location. These fused solutions correspond to i) individual best solution, ii) individual average solution, iii) Fusion-SW solution, iv) Fusion-TE solution, and v) Fusion-CW solution. Individual best and individual average solutions are obtained by selecting the best sensor solution or simply averaging the individual solutions across the nine sensors.

TABLE VI
Sensor Locations and Heading for Wedge Flank Formation

Sensor	GPS-East (m)	GPS-North (m)	Heading (deg)
SW1	283147	4709413	35
SW2	283134	4709443	40
SW3	283165	4709401	31
UGS1	283133	4709431	39
UGS2	283195	4709396	26
UGS3	283156	4709413	34
VM1	283127	4709432	40
VM2	283182	4709394	28
VM3	283184	4709384	26

6.1.1. Scenario 1: Wedge flank formation

The sensor locations and headings corresponding to the wedge flank formation are given in Table VI. After receiving the shot data, each sensor estimates the shooter location relative to its position. This relative solution, in terms of range and bearing, is then relayed to the central node along with the GPS measurements of the sensor locations and the sensor heading (see Table VI). Sensors also provide weights, which indicate the estimated accuracy level of the relative solution, along with its relative solution estimates. After receiving the measurements from the sensors, the central node combines the individual solutions to yield the fused solution.

Figure 8 shows the relative performance between the fusion schemes using the different weighting schemes mentioned previously. In Fig. 8(a), the fusion results obtained from consistency-based weighting scheme (Fusion-CW) is compared against the fusion results obtained from sensor-provided weighting scheme (Fusion-SW) and the individual average. Individual average is the simplest form of fusion, where the fused result is obtained by simply averaging the individual solutions. Figure 8(a) indicates that the fusion results obtained from consistency-based weighting scheme are within the 20 m error circle while the fusion results obtained from sensor-provided weighting scheme and the individual average are mostly outside the 20 m error circle. Figure 8(a) also indicates that the individual average estimates are strongly biased with a T_x -error of 20 m and a T_y -error of 10 m. This bias is clearly visible in the Fusion-SW and Fusion-CW results.

Figure 8(b) contains the histogram of the fusion error for scenario one, shooter position one. Besides the fusion results obtained using the three different weighting schemes mentioned earlier, Fig. 8(b) also contains the results from individual average and individual best. In the individual best approach, the fused solution is the one with the least error, i.e., most accurate. Note that this approach requires knowing the true shooter position a priori and thus it is not feasible in reality. It is important to note that the fusion results obtained from true error based weighting scheme (Fusion-TE) is more accurate than the individual best sensor as shown in Fig. 8(b).

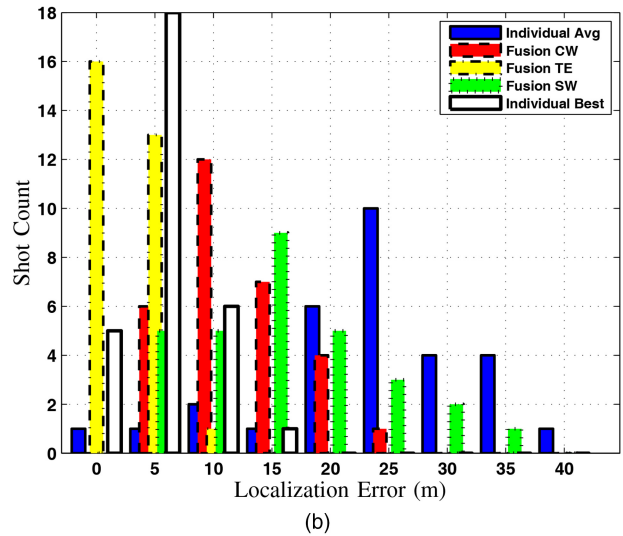
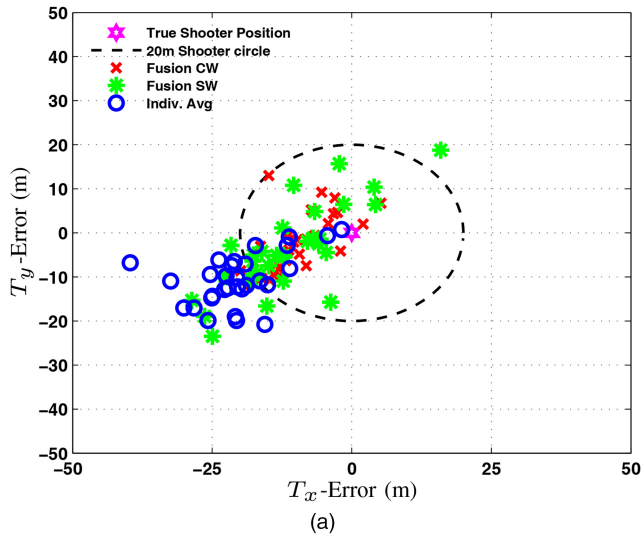


Fig. 8. Fusion result: Scenario 1, shooter position 1. (a) Fusion error. (b) Fusion error histogram.

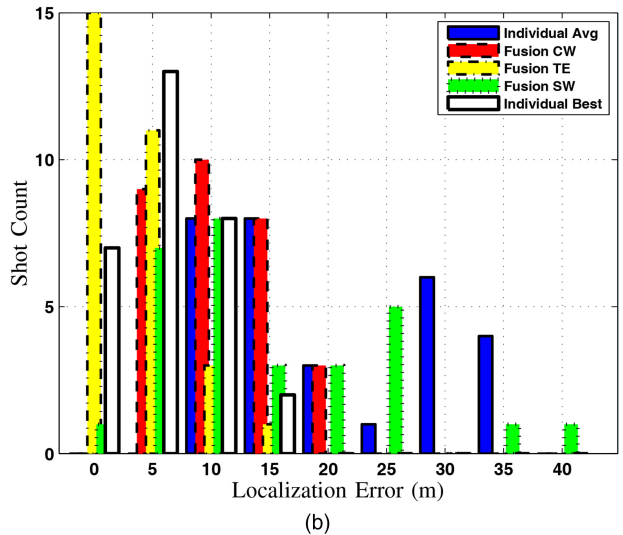
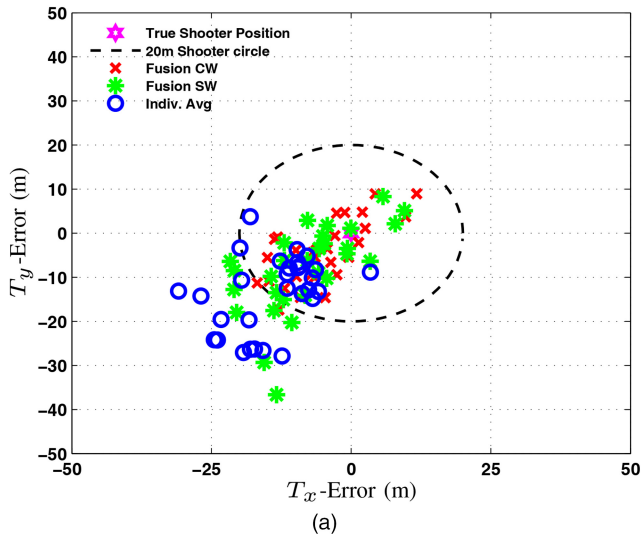


Fig. 9. Fusion result: Scenario 1, shooter position 2. (a) Fusion error. (b) Fusion error histogram.

Fused solution obtained from Fusion-TE yields a zero estimation error 16 out of 30 times while the individual best only has 5 out of 30 solutions with a zero estimation error. The fused solution obtained from individual average is the least accurate with 20 out of 30 solutions with an estimation error of 25 m or higher. Compared to the individual average, the Fusion-SW yields a more accurate solution. In contrast to the results obtained for the numerical simulation, estimation errors are not Gaussian as indicated by Fig. 8(b) except for the error obtained from Fusion-TE.

Figure 9 shows the relative performance across the different fusion schemes for the scenario one, shooter position two. In Fig. 9(a), the fusion results obtained from Fusion-CW is compared against the results obtained from Fusion-SW and the individual average. Compared to shooter position one, these results are less biased, as indicated in Fig. 9(a). As shown in Fig. 9(a), the individual average is biased with a T_x and T_y -errors

of approximately 8 m. Figure 9(a) also indicates that the fusion results obtained from Fusion-CW is within the 20 m error circle while the results obtained from Fusion-SW and the individual average are mostly outside the 20 m error circle. Figure 9(b) contains the histogram of the fusion error for scenario one, shooter position two. Figure 9(b) indicates that the fusion results obtained from Fusion-TE yields a perfect localization 50% of time, i.e., 15 shots out of 30 result in a fused solution with zero error. The fused results obtained from Fusion-SW contains two solutions with errors of 35 and 40 m. Clearly, the fusion results obtained from Fusion-TE is more accurate than the rest of the solutions, as shown in Fig. 9(b).

Figure 10 shows the relative performance across the different fusion schemes for the scenario one, shooter position three. Compared to previous two shooter positions, shooter position three yields the least accurate measurements due to the increased firing dis-

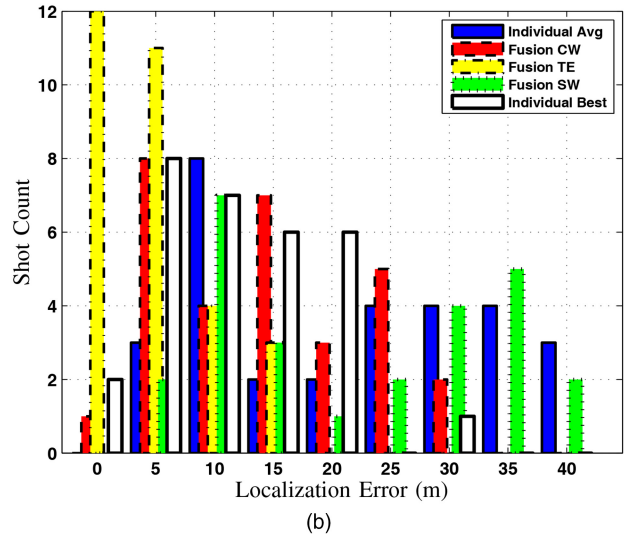
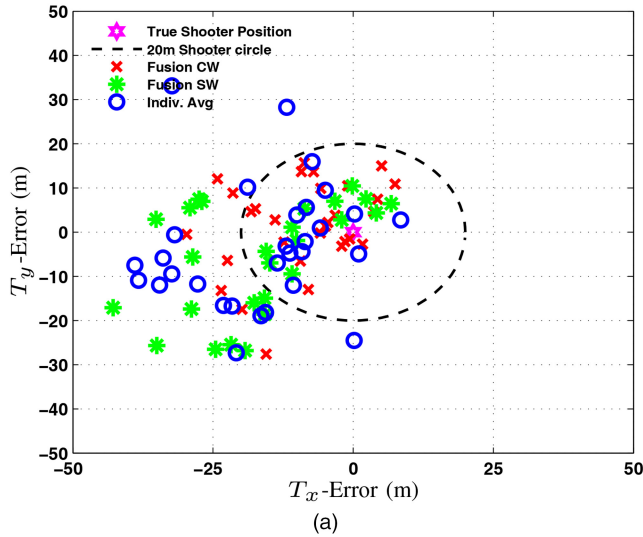


Fig. 10. Fusion result: Scenario 1, shooter position 3. (a) Fusion error. (b) Fusion error histogram.

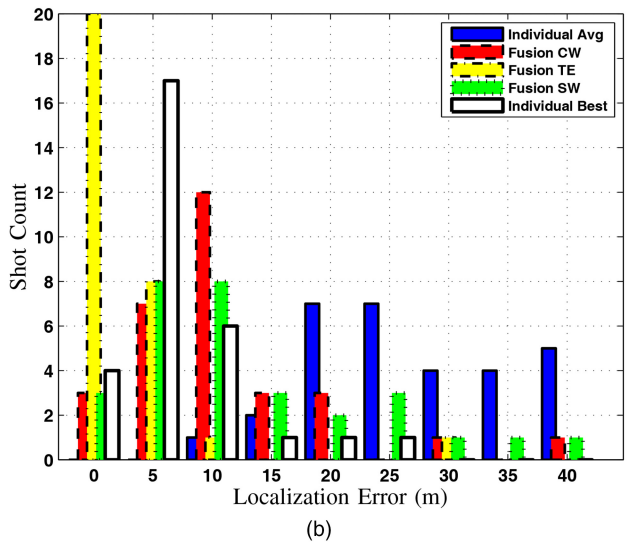
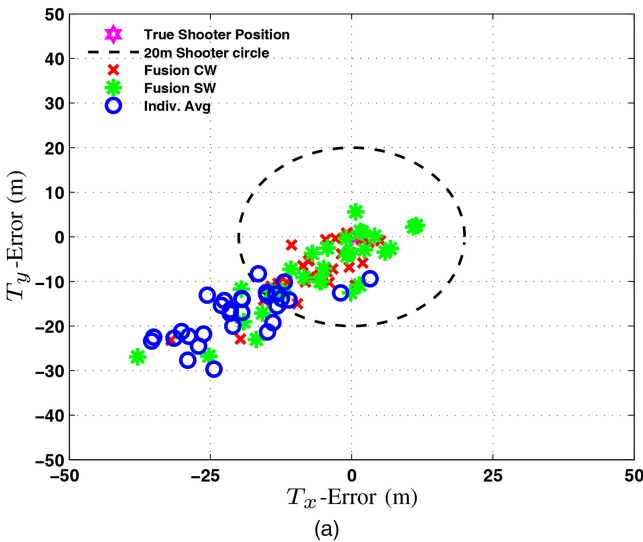


Fig. 11. Fusion result: Scenario 2, shooter position 1. (a) Fusion error. (b) Fusion error histogram.

tance of 300 m. Figure 10(a) compares the fusion results obtained from Fusion-CW against the results obtained from Fusion-SW and the individual average. Figure 10(a) indicates that the majority of fusion results obtained from Fusion-CW, as well as the results obtained from Fusion-SW and the individual average are outside the 20 m error circle. This degradation in performance compared to the previous two shooter positions might be due to the increased firing distance. Figure 10(b) contains the histogram of the fusion error for scenario one, shooter position three. Here also, the fusion results obtained from Fusion-TE is more accurate than the individual best sensor as shown in Fig. 10(b). Finally, note that the accuracy of the results from Fusion-SW is greatly influenced by the individual outliers while the results from Fusion-TE are insensitive to the outliers.

6.1.2. Scenario 2: Quad symmetric formation

This subsection presents the results obtained from scenario two, the quad symmetric sensor formation. Compared to previous scenario, the sensors are more clustered together in this scenario, and therefore, there is a higher level of consistency between the sensors. This higher consistency results in better localization accuracy, as indicated here. The sensor locations and headings correspond to the quad symmetric formation are given in Table VII. Here also, 30 shots were fired for each shooter position, 10 shots per weapon.

Figure 11 shows the relative performance across the fusion schemes using the different weighting schemes. In Fig. 11(a), the fusion results obtained from Fusion-CW are compared against the fusion results obtained from Fusion-SW and the individual average. Figure 11(a) indicates that the fusion results obtained from Fusion-CW and Fusion-SW are mostly within the 20 m

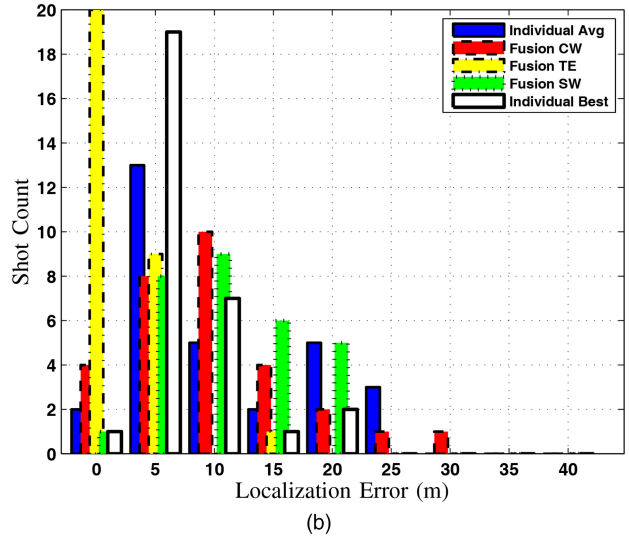
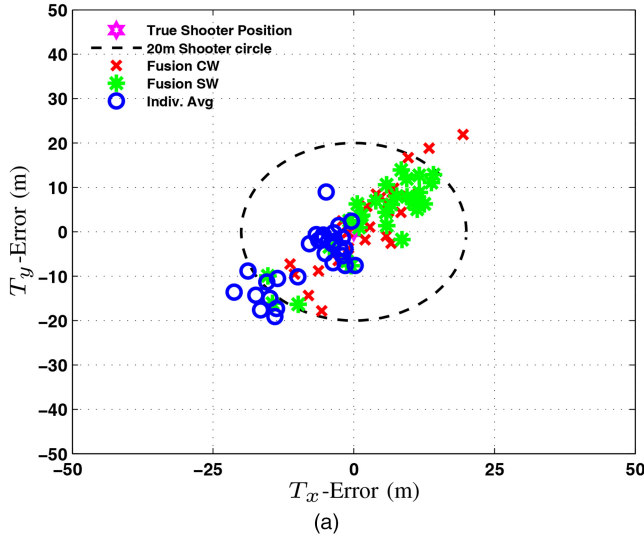


Fig. 12. Fusion result: Scenario 2, shooter position 2. (a) Fusion error. (b) Fusion error histogram.

TABLE VII
Sensor Locations and Heading for Quad Symmetric Formation

Sensor	GPS-East (m)	GPS-North (m)	Heading (deg)
SW1	283130	4709427	40
SW2	283129	4709434	39
SW3	283165	4709401	31
UGS1	283133	4709431	39
UGS2	283169	4709398	30
UGS3	283168	4709405	31
VM1	283127	4709431	40
VM2	283172	4709402	30
VM3	283177	4709395	29

error circle and they are more accurate compared to the individual average. Also note that Fig. 11(a) does not display the strong bias we observed in Fig. 8(a) and the majority of the fused results obtained from Fusion-CW and Fusion-SW shows a less than 10 m error.

Figure 11(b) contains the histogram of the fusion error for scenario two, shooter position one. Besides the fusion results obtained using the three different weighting scheme mentioned earlier, Fig. 11(b) also contains the results from individual average and individual best. Figure 11(b) indicates that the fusion results obtained from Fusion-TE yields a perfect localization two out of three time, i.e., 20 shots out of 30 shots results in a fused solution with zero error. Clearly, the fusion results obtained from Fusion-TE is more accurate than the individual best sensor as shown in Fig. 11(b). Also, note that the results obtained from Fusion-CW are more accurate compared to Fusion-SW, and both Fusion-CW and Fusion-SW yield better results compared to the individual average. Comparing Figs. 8(b) and 11(b) clearly indicates that the results obtained for the quad formation yield better results.

Figure 12 shows the relative performance across the different fusion schemes for the scenario two, shooter position two. In Fig. 12(a), the fusion results obtained

from Fusion-CW are compared against the results obtained from Fusion-SW and the individual average. Figure 12(a) indicates that the fusion results obtained from Fusion-SW, Fusion-CW, and the individual average are mostly within the 20 m error circle or within the close proximity of the error circle. Figure 12(b) contains the histogram of the fusion error for scenario two, shooter position two. Here also, the histogram indicates that the fusion results obtained from Fusion-TE yields a perfect localization two out of three times, i.e., 20 shots out of 30 shots result in a fused solution with zero error. Clearly, the fusion results shown in Fig. 12 are more accurate compared to rest of the results presented here. This high level of accuracy is due to two reasons: i) the clustered quad symmetric sensor formation and ii) the bullet trajectory with sensors distributed on both sides of the trajectory to reduce the miss-distance.

Figure 13 shows the relative performance across the different fusion schemes for the scenario two, shooter position three. Figure 13(a), compares the fusion results obtained from Fusion-CW against the results obtained from Fusion-SW and the individual average. Figure 13(a) indicates that the fusion results obtained from Fusion-CW are mostly within or around the vicinity of the 20 m error circle while the results obtained from Fusion-SW and the individual average are outside the 20 m error circle. Figure 13(b) contains the histogram of the fusion error for scenario two, shooter position three. Note that the fusion results obtained from Fusion-TE are perfect more than 50% of the time and they are more accurate than the individual best sensor, as shown in Fig. 13(b). The performance degradation shown in Fig. 13 is similar to that obtained in Fig. 10 and is due to the increased firing distance compared to the previous two shooter positions. Also note that the performance degradation in Fig. 13 is slightly less than the one observed in Fig. 10 due to the quad symmetric sensor formation.

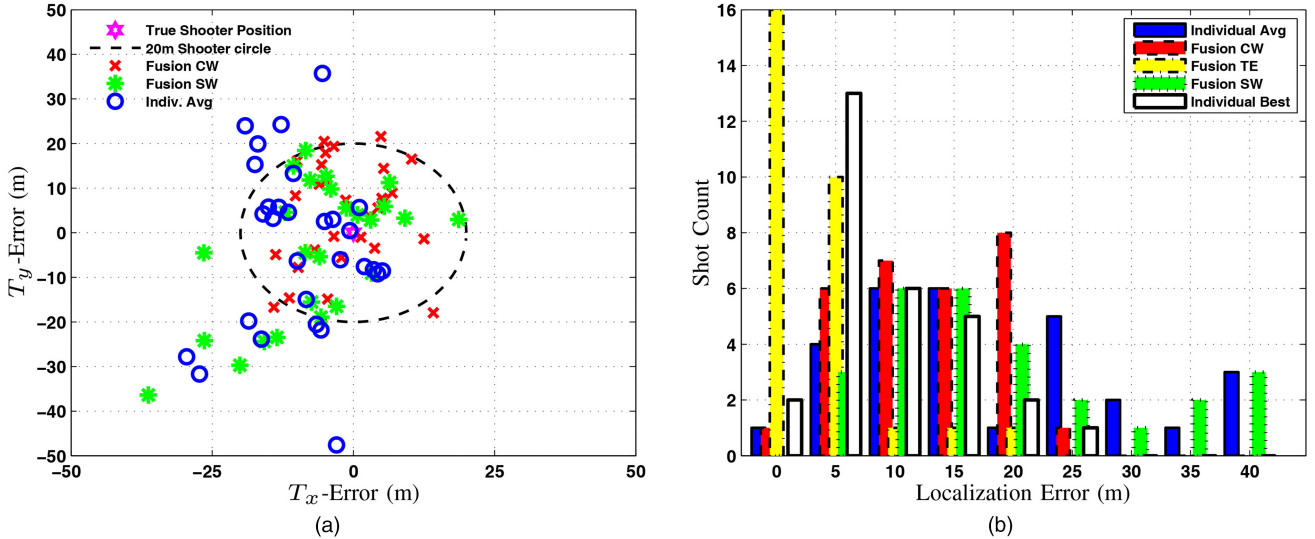


Fig. 13. Fusion result: Scenario 2, shooter position 3. (a) Fusion error. (b) Fusion error histogram.

TABLE VIII
Summary of Fusion Results

Scenario & Shooter Position	Fusion-TE Error (m)	Fusion-CW Error (m)	Fusion-SW Error (m)	Indiv. Avg Error (m)	Indiv. Best Error (m)
Scenario 1 Shooter 1	2.9	12.1	16.3	23.3	6.0
Scenario 1 Shooter 2	3.5	10.7	14.5	20.6	6.0
Scenario 1 Shooter 3	5.0	14.2	21.9	21.9	11.8
Scenario 2 Shooter 1	3.3	11.0	13.2	26.9	6.6
Scenario 2 Shooter 2	2.7	9.7	11.1	10.8	6.7
Scenario 2 Shooter 3	3.4	13.1	20.6	19.1	9.4

Given in Table VIII is the summary of average (averaged across 30 shots) localization error obtained for six different experiments using the five different fusion schemes explained earlier. As expected, the results obtained from Fusion-TE outperform the individual best, and on average the Fusion-CW yields better results compared to Fusion-SW. Also note that the Fusion-CW and Fusion-SW yield better results compared to the individual average except for scenario two, shooter positions two and three. For scenario two, shooter positions two and three, the results obtained from individual average are slightly better than Fusion-SW. This is due to the fact that the clustered sensors within the quad symmetric formation yield consistent measurements, which are equally distributed around the truth, and weighting them equally yields better results compared to using inconsistent weights. The consistency-based weighting scheme presented here is just one of the ad hoc approaches to develop synthetic weights. Numerous other schemes exist based on the consistency test that we are currently pursuing in an attempt to achieve the performance of Fusion-TE.

7. CONCLUSIONS

The shooter localization problem using a network of soldier-worn gunfire detection systems is considered here. This paper presents a fusion algorithm that utilizes

the benefits of the sensor network layout of all the sensors within a small combat unit to help refine shooter localization accuracy. Main contributions of this work include (i) a detailed formulation of the fusion methodology and its performance analysis through numerical simulations; (ii) parameter reduction of the optimization problem and a consistency-based weighting scheme for the real-time implementation of the fusion algorithm; and (iii) detailed experimental results and the analysis of data. It is shown that the multi-sensor fusion algorithm for soldier-worn gunfire detection systems is essentially the weighted nonlinear least-squares algorithm, which can be easily implemented using the Gauss-Newton method. Since the GPS accuracy of the sensors is much higher compared to the shooter localization accuracy, it is also shown that accepting the GPS measurements as ground truth for the sensor locations and simply estimating the shooter location greatly reduce the dimensionality of the optimization problem and thus decrease the computational cost without sacrificing performance accuracy. The numerical results given in Section 5 indicate that the fusion algorithm is able to improve the localization accuracy by a factor of four compared to the simple averaged solution, if the underlying assumptions are valid and the weights associated with individual sensor locations are consistent. Despite the lack of consistency in the weights provided by the sensors, the

fusion algorithm along with the proposed consistency-based weighting scheme is able to produce a fused solution twice as accurate as the simple individual average solution.

Though the proposed fusion approach was able to yield desirable results, there are several aspects of the proposed approach that can be further improved. Few of those features are (i) an improved weighting scheme that would yield a fused solution that approaches the accuracy obtained from the true error based weighting scheme, (ii) a mathematically rigorous method to quantify the uncertainties associated with the maximum likelihood estimates, and (iii) an investigation of the performance gain in fusing raw sensor measurements, such as the two direction of arrival angles and the time difference of arrival between the muzzle blast and the shockwave versus the relative shooter position.

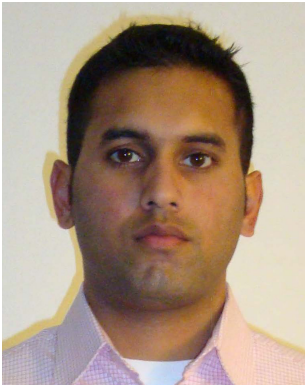
ACKNOWLEDGMENT

This work is conducted in collaboration with the U.S. Army Natick Soldier Research Development & Engineering Center (NSRDEC) and the U.S. Army Armament Research, Development and Engineering Center (ARDEC). Authors would like to acknowledge Bruce Buckland from NSRDEC, Sachi Desai and George Cakiades from ARDEC for their support.

REFERENCES

- [1] J. Ash, G. Whipps, and R. Kozick
Performance of shockwave-based shooter localization under model misspecification.
In IEEE International Conference on Acoustics Speech and Signal Processing (ICASSP), Dallas, TX, Mar. 2010, pp. 2694–2697.
- [2] J. Bédard and S. Paré
Ferret: A small arms' fire detection system: Localization concepts.
In Proceedings of Society of Photo-Optical Instrumentation Engineers (SPIE) Conference, vol. 5071, Orlando, FL, Apr. 2003, pp. 497–509.
- [3] G. Cakiades, S. Desai, S. Deligeorges, B. E. Buckland, and J. George
Fusion solution for soldier wearable gunfire detection systems.
In Proceedings of SPIE: Defence, Security, and Sensing, Baltimore, MD, Apr. 23–27, 2012.
- [4] J. L. Crassidis and J. L. Junkins
Optimal Estimation of Dynamic System.
Boca Raton, FL: Chapman & Hall/CRC, 2004, ch. 1.
- [5] T. Damarla, L. Kaplan, and G. Whipps
Sniper localization using acoustic asynchronous sensors.
Sensors Journal, IEEE, **10**, 9 (Sept. 2010), 1469–1478.
- [6] E. Danicki
The shock wave-based acoustic sniper localization.
Nonlinear Analysis: Theory, Methods & Applications, **65**, 5 (2006), 956–962.
- [7] G. L. Duckworth, D. C. Gilbert, and J. E. Barger
Acoustic counter-sniper system.
In Proceedings of Society of Photo-Optical Instrumentation Engineers (SPIE) Conference, vol. 2938, Boston, MA, Nov. 1997, pp. 262–275.
- [8] P. Fishbane, S. Gasiorowicz, and S. Thornton
Physics for Scientists and Engineers, (2nd ed.).
Upper Saddle River, NJ: Prentice Hall, 1996, vol. 1, ch. 14, pp. 398–399.
- [9] J. George, L. M. Kaplan, R. Kozick, and S. Deligeorges
Multi-sensor data fusion using soldier-worn gunfire detection systems.
In Proceedings of MSS Battlespace Acoustic and Magnetic Sensors (BAMS), Washington, D.C., Oct. 2011.
- [10] J. George and L. Kaplan
Shooter localization using soldier-worn gunfire detection systems.
In Proceedings of the 12th International Conference on Information Fusion (FUSION), Chicago, IL, July 2011, pp. 1–8.
- [11] L. M. Kaplan and Q. Le
On exploiting propagation delays for passive target localization using bearings-only measurements.
Journal of the Franklin Institute, **342**, 2 (Mar. 2005), 193–211.
- [12] L. Kaplan, T. Damarla, and T. Pham
QoI for passive acoustic gunfire localization.
In 5th IEEE International Conference on Mobile Ad Hoc and Sensor Systems (MASS), Atlanta GA, Sept.–Oct. 2008, pp. 754–759.
- [13] R. Kozick, J. George, L. M. Kaplan, and S. Deligeorges
Centralized fusion of acoustic sensor data for gunfire localization.
In Proceedings of MSS Battlespace Acoustic and Magnetic Sensors (BAMS), Washington, D.C., Oct. 2011.
- [14] R. Kozick, G. Whipps, and B. Sadler
Accuracy and tradeoff analysis of sniper localization systems with a network of acoustic sensors.
In Proceedings MSS Battlespace Acoustics & Seismic Sensing, Magnetic & Electric Field Sensors, Laurel, MD, Aug. 2009.
- [15] P. Kuckertz, J. Ansari, J. Riihijarvi, and P. Mahonen
Sniper fire localization using wireless sensor networks and genetic algorithm based data fusion.
In IEEE Military Communications Conference (MILCOM 2007), Orlando, FL, Oct. 2007, pp. 1–8.
- [16] A. Ledeczki, P. Volgyesi, M. Maroti, G. Simon, G. Balogh, A. Nadas, B. Kusy, S. Dora, and G. Pap
Multiple simultaneous acoustic source localization in urban terrain.
In Fourth International Symposium on Information Processing in Sensor Networks (IPSN), Los Angeles, CA, Apr. 2005, pp. 491–496.
- [17] A. Ledeczki, A. Nadas, P. Volgyesi, G. Balogh, B. Kusy, J. Sallai, G. Pap, S. Dora, K. Molnar, M. Maroti, and G. Simon
Countersniper system for urban warfare.
ACM Transactions on Sensor Networks, **1** (Nov. 2005), 153–177.
- [18] P. Li and X. Ma
Robust acoustic source localization with tdoa based ransac algorithm.
In Emerging Intelligent Computing Technology and Applications, ser. Lecture Notes in Computer Science, Springer Berlin/Heidelberg, 2009, vol. 5754, pp. 222–227.
- [19] D. Lindgren, O. Wilsson, F. Gustafsson, and H. Habberstad
Shooter localization in wireless sensor networks.
In Proceedings of the 12th International Conference on Information Fusion (FUSION), Seattle, WA, July 2009, pp. 404–411.
- [20] D. Lindgren, O. Wilsson, F. Gustafsson, and H. Habberstad
Shooter localization in wireless microphone networks.
EURASIP Journal on Advances in Signal Processing, **2010**, 6 (Feb. 2010), 1–25.

- [21] J. Liu, J. Reich, and F. Zhao
Collaborative in-network processing for target tracking.
EURASIP Journal on Applied Signal Processing, **2003**, 4
(Jan. 2003), 378–391.
- [22] R. Maher
Modeling and signal processing of acoustic gunshot recordings.
In *Digital Signal Processing Workshop, 12th-Signal Processing Education Workshop*, 4th, Teton National Park, WY, Sept. 2006, pp. 257–261.
- [23] T. Makinen and P. Pertila
Shooter localization and bullet trajectory, caliber, and speed estimation based on detected firing sounds.
Applied Acoustics, **71**, 10 (2010), 902–913.
- [24] M. Maroti, G. Simon, A. Ledeczki, and J. Sztipanovits
Shooter localization in urban terrain.
Computer, **37**, 8 (Aug. 2004), 60–61.
- [25] J. M. Mendel
Lessons in Digital Estimation Theory.
Englewood Cliffs, NJ: Prentice-Hall, Inc., 1987.
- [26] J. Millet and B. Balingand
Latest achievements in gunfire detection systems.
In *Meeting Proceedings RTO-MP-SET-107, Battlefield Acoustic Sensing for ISR Applications*, NeuillysurSeine, France, Oct. 2006, pp. 1–14.
- [27] J. A. Nelder and R. Mead
A simplex method for function minimization.
The Computer Journal, **7**, 4 (1965), 308–313.
- [28] R. Stoughton
Measurements of small-caliber ballistic shock waves in air.
The Journal of the Acoustical Society of America, **102**, 2
(Aug. 1997), 781–787.
- [29] R. B. Stoughton
SAIC SENTINEL acoustic counter-sniper system.
In *Proceedings of Society of Photo-Optical Instrumentation Engineers (SPIE) Conference*, vol. 2938, Boston, MA, Nov. 1997, pp. 276–284.
- [30] R. Osborne, III, Y. Barshalom, J. George, and L. Kaplan
Statistical efficiency of simultaneous target and sensors location with position dependent noise.
In *Proceedings of SPIE: Defence, Security, and Sensing*, Baltimore, MD, Apr. 23–27, 2012.
- [31] G. Vakulya and G. Simon
Fast adaptive acoustic localization for sensor networks.
IEEE Transactions on Instrumentation and Measurement, **60**, 5 (May 2011), 1820–1829.
- [32] P. Volgyesi, G. Balogh, A. Nadas, C. B. Nash, and A. Ledeczki
Shooter localization and weapon classification with soldier-wearable networked sensors.
In *Proceedings of the 5th International Conference on Mobile Systems, Applications and Services*, New York, NY, June 2007, pp. 113–126.



Jemin George received his B.S. (2005), M.S. (2007), and Ph.D. (2010) in aerospace engineering from the State University of New York at Buffalo.

In 2008, he was a summer research scholar with the U.S. Air Force Research Laboratory's Space Vehicles Directorate at Kirtland Air Force Base in Albuquerque, NM. He was a National Aeronautics and Space Administration Langley Aerospace Research Summer Scholar with the Langley Research Center in 2009. From 2009–2010 he was a research fellow with the Stochastic Research Group, Department of Mathematics, Technische Universitat Darmstadt, Darmstadt, Germany. He is currently with the Networked Sensing & Fusion Branch of the U.S. Army Research Laboratory. His principal research interests include stochastic systems, control theory, nonlinear filtering, information fusion, and target tracking.

Lance M. Kaplan received his B.S. degree with distinction from Duke University, Durham, NC, in 1989 and his M.S. and Ph.D. degrees from the University of Southern California, Los Angeles, in 1991 and 1994, respectively, all in electrical engineering.

From 1987–1990, he worked as a technical assistant at the Georgia Tech Research Institute. He held a National Science Foundation Graduate Fellowship and a USC Dean's Merit Fellowship from 1990–1993, and worked as a research assistant in the Signal and Image Processing Institute at the University of Southern California from 1993–1994. Then, he worked on staff in the Reconnaissance Systems Department of the Hughes Aircraft Company from 1994–1996. From 1996–2004, he was a member of the faculty in the Department of Engineering and a senior investigator in the Center of Theoretical Studies of Physical Systems (CTSPS) at Clark Atlanta University (CAU), Atlanta, GA. Currently, he is a researcher in the Networked Sensing and Fusion branch of the U.S. Army Research Laboratory. Dr. Kaplan serves as editor-in-chief for the *IEEE Transactions on Aerospace and Electronic Systems* (AES). In addition, he also serves on the Board of Governors of the IEEE AES Society and on the Board of Directors of the International Society of Information Fusion. He is a three time recipient of the Clark Atlanta University Electrical Engineering Instructional Excellence Award from 1999–2001. His current research interests include signal and image processing, automatic target recognition, information/data fusion, and resource management.

